Article

Not peer-reviewed version

Response of Grassland Vegetation Growth to Drought in Inner Mongolia of China from 2002 to 2020

Anzhou Zhao * , Ruihao Xu , Lidong Zou , Xiufang Zhu

Posted Date: 2 October 2023

doi: 10.20944/preprints202310.0075.v1

Keywords: Vegetation indexes; GOSIF; GPP; Drought events; Inner Mongolia grassland

Article

Response of Grassland Vegetation Growth to Drought in Inner Mongolia of China from 2002 to 2020

Anzhou Zhao [1,*], Ruihao Xu [1], Lidong Zou [2] and Xiufang Zhu [3]

[1] School of Mining and Geomatics Engineering, Hebei University of Engineering, Handan 056038, China
[2] School of Artificial Intelligence, Shenzhen Polytechnic University, Shenzhen 518055, China
[3] State Key Laboratory of Remote Sensing Science, Jointly Sponsored by Beijing Normal University and Institute of Remote Sensing and Digital Earth of Chinese Academy of Sciences, Beijing 100875, China
* Correspondence: zhaoanzhou@126.com; Tel.: +860310 8579519; Fax: +860310 8579519

Abstract: Drought poses a significant environmental risk and can deeply affect the growth of grasslands. However, there is still uncertainty regarding the precise impact of varying levels of drought on grassland growth. To address this gap, we utilized several key indicators, including the Normalized Difference Vegetation Index (NDVI), Enhanced Vegetation Index (EVI), the Global Orbiting Carbon Observatory-2 based Solar-induced Chlorophyll Fluorescence (GOSIF), and the Gross Primary Productivity (GPP), in conjunction with drought indices (the Standardized Precipitation Evapotranspiration Index (SPEI) and the soil moisture (SM). Our study aimed to comprehensively assess the consistency of spatio-temporal patterns in grassland vegetation and its responsiveness to different drought levels in the Inner Mongolia region from 2002 to 2020. Results indicated that NDVI, EVI, GOSIF, and GPP in grassland vegetation across Inner Mongolia exhibited significant increasing trends from 2002 to 2020. Specifically, NDVI, EVI, GOSIF, and GPP all displayed consistent spatial patterns, with 25.83%, 21.18%, 22.65% and 48.13% of the grassland area showing significant increases, respectively. Drought events, as described by SPEI and SM, in June 2007 to September 2007 and June 2017 to July 2017, were selected to evaluated the response of grassland vegetation to drought. The drought events of 2007 and 2017 resulted in reductions in NDVI, EVI, GOSIF, and GPP relative to multi-year average (2002-2020). GOSIF exhibited a more intense response to drought, suggesting that GOSIF may reflect the inhibition of water stress on grassland photosynthesis better than NDVI and EVI during drought in 2007 and 2017. The reductions in NDVI, EVI, GOSIF and GPP in grassland increased significantly across different drought-levels, with the sharpest reductions observed during extreme drought. Under the severe and extreme drought events, the most substantial reductions in NDVI, EVI, GOSIF, and GPP were observed in the temperate steppe (TS). Moreover, the effects of different drought severity levels within the same grassland type varied, with the most significant reductions in NDVI, EVI, GOSIF and GPP observed during extreme drought. Our results provide new perspectives for developing and implementing effective strategies to address grassland carbon cycling management and climate change in Inner Mongolia.

Keywords: vegetation indexes; GOSIF; GPP; drought events; Inner Mongolia grassland

1. Introduction

Drought is a common hydrometeorological phenomenon and a significant environmental risk that increases vegetation mortality and reduces vegetation productivity [1–4]. For the past several decades, the frequency and severity of drought events have shown a rapidly increasing trend with temperature rising [5–7]. Earth system models also project a vast expansion of regions often affected by extreme and severe droughts in the coming decades [8,9]. Grassland areas cover approximately 25% of the Earth's land surface, yet they store approximately 34% of global terrestrial carbon storage [10–12]. Grasslands are among the most fragile ecosystems and are highly susceptible to droughts [10,11]. Recently, some research have indicated that drought is recognized as the key forcing on grassland ecosystem dynamics [10,11,13]. Therefore, it is important to study the response of grassland vegetation growth to drought under the background of global warming.

Preprints (www.preprints.org) | NOT PEER-REVIEWED | Posted: 2 October 2023 doi:10.20944/preprints202310.0075.v1

Remote sensing observations have proven to be invaluable in monitoring drought characteristics and quantifying its impact on grasslands over varying time intervals and spatial scales [14,15]. Recently, remote sensing approaches have developed and widely applied vegetation indices (e.g.; the Normalized Difference Vegetation Index (NDVI), the Enhanced Vegetation Index (EVI), Near-Infrared Reflectance of Vegetation (NIRv)) and drought indices (e.g.; the Temperature-Vegetation Dryness Index (TVDI), the Soil Water Deficit Index (SWDI), the Standardized Precipitation Evapotranspiration Index (SPEI), etc.) to assess the effects of drought events on grassland ecosystems [3,16]. Traditionally used vegetation indices (such as NDVI, EVI and NIRv) do not directly reflect changes in actual photosynthesis in grassland ecosystems when water stress occurs [11,17,18]. Some studies have also used Solar-induced Chlorophyll Fluorescence (SIF) to monitor vegetation response to drought events at different spatial and temporal scales [11,16,19,20]. Unlike traditional vegetation indices, SIF is directly related to the actual photosynthetic function of plants and can reveal rapid changes in water stress within the vegetation canopy [21,22]. However, the degree of change in photosynthesis or productivity is highly sensitive to different drought-levels [10,23]. Generally, extreme and severe drought events can result in additional reductions in grassland photosynthesis or productivity due to increased mortality and physiological function recession [23]. Previous studies have primarily focused on the effect of specific drought levels on grassland, leaving the response of grassland ecosystems to different intensities of drought largely unexplored. Moreover, different types of grassland ecosystems exhibit varying responses to droughts. Therefore, a more precise investigation into the spatiotemporal evolution patterns of grassland ecosystems and their response to different drought-levels is warranted.

Inner Mongolia is highly responsive to global climate change, with more than 74% of its area covered by various types of grasslands [24,25]. This region has experienced increased temperatures, reduced precipitation, and more frequent droughts over the past few decades [25]. Understanding the spatial and temporal patterns of grassland NDVI, EVI, GOSIF, and GPP and their responses to different drought-levels in Inner Mongolia is of great significance for enhancing ecological security in Northern China [25]. The primary objective of this study was to quantify the spatiotemporal variation in the characteristics of grassland ecosystems and their response to different intensities of drought in Inner Mongolia over the past two decades (2002-2020) using NDVI, EVI, GOSIF, GPP, SPEI and soil moisture (SM) data. Additionally, we assessed variation in NDVI, EVI, GOSIF, and GPP losses in different grassland types under the same drought severity levels. This study aimed to answer the following questions: (1) What are spatial and temporal patterns in the characterization of Inner Mongolia grasslands, such as NDVI, EVI, GOSIF and GPP? (2) To what extent do typical drought events influence grassland ecosystems in Inner Mongolia? (3) How do NDVI, EVI, GOSIF, and GPP reductions vary in different grassland biomes under different drought levels? Our results provide a more robust and less the uncertain understanding by applying a single data source and scientific basis to examine grassland ecosystems' responses to droughts at various levels.

2. Materials and Methods

2.1. Study area

The Inner Mongolia, situated between 37° 24′N to 53° 23′N and 97° 12′E to 126° 04′E, is located in northern China and covers an expansive area of approximately 118.3×10^4 km^2. The topography is characterized as long and narrow, with elevations decreasing from the southwest to the northeast (Figure 1). Influenced significantly by the Asia monsoon, Inner Mongolia is a typical temperate continental monsoon climate. Consequently, the mean annual rainfall varies from 50 to 550 mm and diminishes from the northeast to the southwest [24,26,27]. The annual mean temperature typically falls within the range of -4~10℃, and progressively increases from the northeast to the southwest [25–28]. Grasslands dominate the Inner Mongolia landscape, constituting the primary vegetation types and covering approximately 74% of the entire region. Nevertheless, due to the temporal variability of precipitation and the effects of global warming, Inner Mongolia has experienced a heightened frequency droughts over the past decades [13,29].

Preprints (www.preprints.org) | NOT PEER-REVIEWED | Posted: 2 October 2023 doi:10.20944/preprints202310.0075.v1

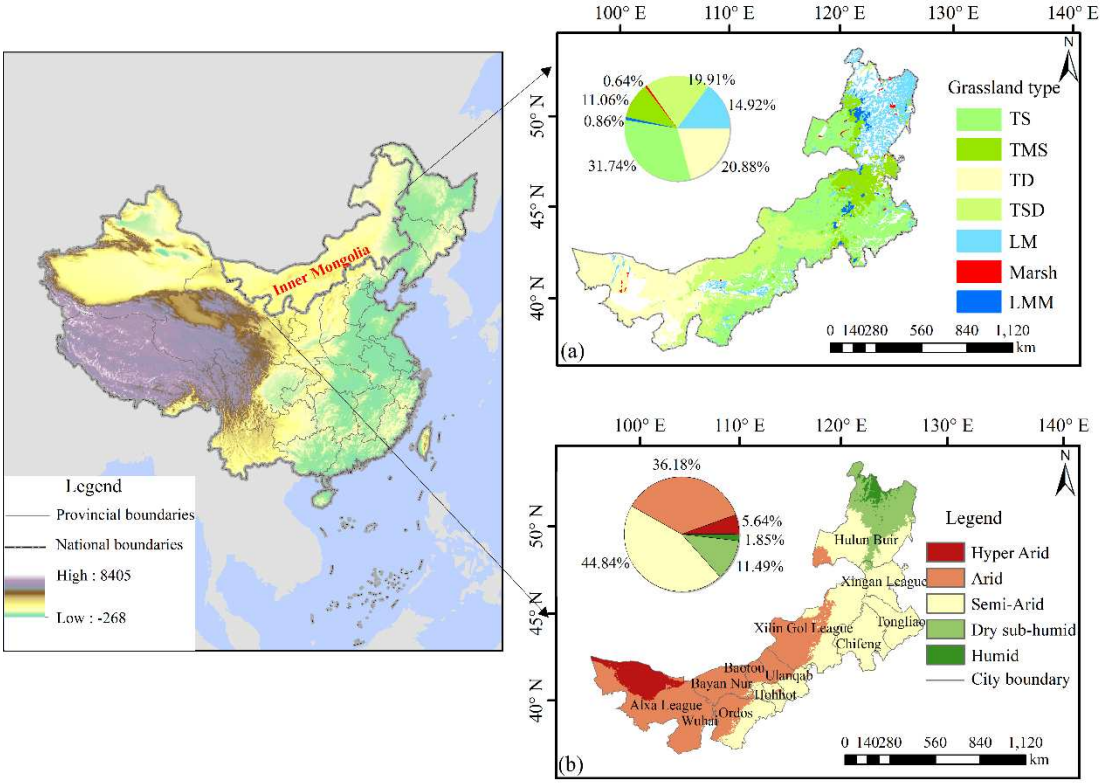

Figure 1. Spatial pattern of grassland types (a) and climate class (b) in Inner Mongolia Autonomous Region of China.

2.2. Data sources and preprocessing

2.2.1. MODIS products

In this study, Moderate Resolution Imaging Spectroradiometer (MODIS) products, specifically NDVI, EVI, and GPP were used to monitor the vegetation because of their high-quality data sources (https://e4ftl01.cr.usgs.gov/). NDVI and EVI obtained used with a1-month temporal resolution and a 0.05°spatial resolution of from the MOD13C2 product. To mitigate the impact of aerosol and atmospheric and molecular scattering, the maximum value composite (MVC) method was used to generate yearly NDVI and EVI datasets [30]. GPP data were sourced from the MOD17A2H product, featuring a temporal resolution of 8-day and a spatial resolution of 500 m. The monthly and yearly GPP data to achieve spatial resolution of 0.05°, starting from 8-day data were synthesized and resampled [31]. The period from 2002 to 2020 was considered in this study.

2.2.2. GOSIF data

A global Orbiting Carbon Observatory-2 (OCO-2) Solar-induced chlorophyll fluorescence (SIF) dataset, known as GOSIF measured in $W \cdot m^{-2} \cdot \mu m^{-1} \cdot sr^{-1}$, covering the period from January 2002 to December 2020 were retrieved from the following website: http://data.globalecology.unh.edu/data/GOSIF_v2/. GOSIF was developed by integrating discrete OCO-2 SIF soundings, remote sensing data from MODIS, and meteorological reanalysis data [32]. It offers global coverage with high spatial and temporal resolutions (0.05°and 8 days). GOSIF has gained widespread use in assessing terrestrial photosynthesis and studying vegetation responses to drought under the background of global climate change [32–34]. In this study, monthly and yearly GOSIF data was used to evaluate its effectiveness in tracking vegetation changes and monitoring drought conditions.

2.2.3. SPEI data

The SPEI dataset was originally proposed by Vicente-Serrano et al. (2010)[35]. It is calculated based on available water (monthly precipitation) and atmospheric evaporation demand (potential evapotranspiration) and offers the advantage of providing multi-time scale data while accounting for potential evapotranspiration in drought assessments [36]. SPEI has been widely used in numerous studies to assess drought trends [23,37,38]. The SPEI version 2.8 is available for access at the following

Preprints (www.preprints.org) | NOT PEER-REVIEWED | Posted: 2 October 2023 doi:10.20944/preprints202310.0075.v1

website: https://digital.csic.es/handle/10261/288226. Considering the SPEI with three-month time scale (SPEI-3) can better reflect the severity and duration of grassland drought [25], SPEI-3 was used to assess the effect of drought events on grassland vegetation growth in Inner Mongolia. The SPEI values and corresponding drought levels were described in Table 1 [35,39].

Table 1. Classification of drought levels based on the SPEI values.

Classification	SPEI value	Status
1	SPEI≥-0.5	No drought
2	-0.5＜SPEI≤-1.0	Mildly drought
3	-1.0＜SPEI≤-1.5	Moderately drought
4	-1.5＜SPEI≤-2.0	Severely drought
5	SPEI≤-2.0	Extreme drought

2.2.4. Soil moisture data

Climate Change Initiative (CCI) SM dataset, which provides surface soil moisture information, is a product of by the European Space Agency (ESA) CCI [40,41]. The latest release (v07.1) spans 43 years from November 1978 to December 2021, and is accessible at this link: https://catalogue.ceda.ac.uk/uuid/. The SM CCI COMBINED dataset, which has a spatial resolution of 0.25°×0.25° and a volumetric unit (m^3/m^3), were selected to assess drought conditions in the Inner Mongolia grassland from 2002 o 2020. The reliability of the dataset has been validated in various regions worldwide [42–44].

2.2.5. Other data

The climate class was characterized by the aridity index (AI), which is computed based on annual precipitation, annual temperature, and annual reference evapo-transpiration (ET0) data from the 1970-2000 period. This dataset is accessible at https://csidotinfo.wordpress.com/data/global-aridity-and-pet-database/. In this study, the Hyper Arid (AI<0.03), Arid (0.03<AI≤0.2), Semi-Arid (0.2<AI≤0.5), Dry sub-humid (0.5<AI≤0.65), and Humid (AI>0.65) were categorized by AI values in Inner Mongolia (Figure 1b) [45,46].

The classification of grassland types in Inner Mongolian of China was obtained from the Inner Mongolian Institute of Grassland Surveying and Planning [47,48]. The Inner Mongolian grassland comprises predominant types, including temperate steppe (TS), temperate meadow-steppe (TMS), temperate desert type (TD), temperate steppe-desert (TSD), lowland meadow (LM), Marsh, and temperate mountain meadow (TMM) (Figure 1a).

2.3. Subsection

2.3.1. Theil-Sen Median trend and M-K test

Theil-Sen Median slope and Mann–Kendall (M-K) nonparametric trend analysis methods were used to assess the change trends in NDVI, EVI, GOSIF, and GPP during the period from 2002 to 2020. This method is favored for their simplicity, computational efficiency, and robustness against data distribution or measurement errors. The calculation of the trend (β) is performed using the following equations [49–51]:

$$\beta = Median(\frac{x_j - x_i}{j - i}), \quad \forall i < j \tag{1}$$

$$S = \sum_{i=1}^{n-1} \sum_{j=i+1}^{n} \mathrm{sgn}(x_j - x_i) \tag{2}$$

$$\mathrm{sgn}(\theta) = \begin{cases} -1 & \mathrm{if}(\theta < 0) \\ 0 & \mathrm{if}(\theta = 0) \\ 1 & \mathrm{if}(\theta > 0) \end{cases} \tag{3}$$

$$Var(S) = \frac{n(n-1)(2n+5)}{18} \tag{4}$$

Preprints (www.preprints.org) | NOT PEER-REVIEWED | Posted: 2 October 2023 doi:10.20944/preprints202310.0075.v1

$$Z=\begin{cases}(S-1)/\sqrt{Var(S)} & S>0\\ 0 & S=0\\ (S+1)/\sqrt{Var(S)} & S<0\end{cases} \quad (5)$$

where β denotes the change trend, n denotes the length of the time series of NDVI, EVI, GOSIF, and GPP, sgn is the sign function, i and j are serial numbers, x_i and x_j denote the values at moments i and j, respectively. β >0 indicates an increasing trend; β <0 indicates a decreasing trend. $|Z|\geq 1.96$ represent the change trend is significant at 0.05 confidence level.

2.3.2. Standardized Anomaly

The calculation standardized anomaly (SA) for each variable at the pixel level during the ith month of a drought period can be performed using the following equation [2,52]:

$$\mathrm{SA}_{\mathrm{grassland}}(i,j)=\frac{\mathrm{Var}(i,j)-\overline{\mathrm{Var}_{2002-2020}(i,j)}}{\sigma(\mathrm{Var}_{2002-2020}(i,j))} \quad (6)$$

where, $\mathrm{SA}_{\mathrm{grassland}}(i,j)$ and $\mathrm{Var}(i,j)$ is the standardized anomaly and value of each variable (CCI-SM, NDVI, EVI, GOSIF, GPP) at the ith grid for the jth month during the drought period, respectively; $\overline{\mathrm{Var}_{2002-2020}(i,j)}$ and $\sigma(\mathrm{Var}_{2002-2020}(i,j))$ is the average and standard deviation of each variable at the ith grid for the jth month during 2002-2020, respectively.

2.3.3. Grassland NDVI, EVI, GOSIF and GPP loss assessment

NDVI, EVI, GOSIF and GPP reductions induced by drought are calculated as the difference between the mean values of NDVI, EVI, GOSIF and GPP during drought years reference years [10].

$$\triangle\mathrm{Var}=\frac{\mathrm{Var}_{\mathrm{drought}}-\mathrm{Var}_{\mathrm{mean}}}{\mathrm{Var}_{\mathrm{mean}}}\times 100 \quad (7)$$

where $\triangle\mathrm{Var}$ represent the percentage reduction in NDVI, EVI, GOSIF and GPP during drought years, $\mathrm{Var}_{\mathrm{drought}}$ and $\mathrm{Var}_{\mathrm{mean}}$ denote the value of NDVI, EVI, GOSIF and GPP during drought years (SPEI-12<-1.0) and near normal years (-1.0<SPEI-12≤1.0), respectively.

3. Results

3.1. Spatio-temporal patterns of NDVI, EVI, GOSIF, and GPP from 2002 to 2020

Figure 2a illustrates the change trends in monthly grassland NDVI and EVI from 2002 to 2020, revealing apparent periodical characteristics with a one-year cycle. Notably, the maximum values of grassland NDVI, reaching around 0.40, consistently occurred in July or August each year, signifying the period when grassland growth and metabolism were most vigorous. Conversely, the minimum values of grassland NDVI, dropped below 0.1, were consistently observed in January, indicating minimal grassland growth during that period. The change trends of monthly grassland EVI exhibited similar patterns to NDVI, but the fluctuation range of EVI values was lower than NDVI (Figure 2a). Monthly grassland GOSIF and GPP also displayed clear periodic characteristics throughout the period from 2002 to 2020 (Figure 2b). GOSIF exhibited patterns similar to those of GPP, with the maximum value appearing in August 2018, reaching 0.1371 $W{\cdot}m^{-2}{\cdot}\mu m^{-1}{\cdot}sr^{-1}$. Conversely, the minimum GOSIF value was recorded in February 2014, with a value of -0.0121 $W{\cdot}m^{-2}{\cdot}\mu m^{-1}{\cdot}sr^{-1}$. In the case of grassland GPP, its maximum value was observed in July 2012, reaching 126.61 $gC{\cdot}m^{-2}{\cdot}month^{-1}$. Overall, the monthly variations grassland NDVI, EVI, GOSIF and GPP consistently exhibited a one year cycle in Inner Mongolia between 2002 and 2020.

Preprints (www.preprints.org) | NOT PEER-REVIEWED | Posted: 2 October 2023 doi:10.20944/preprints202310.0075.v1

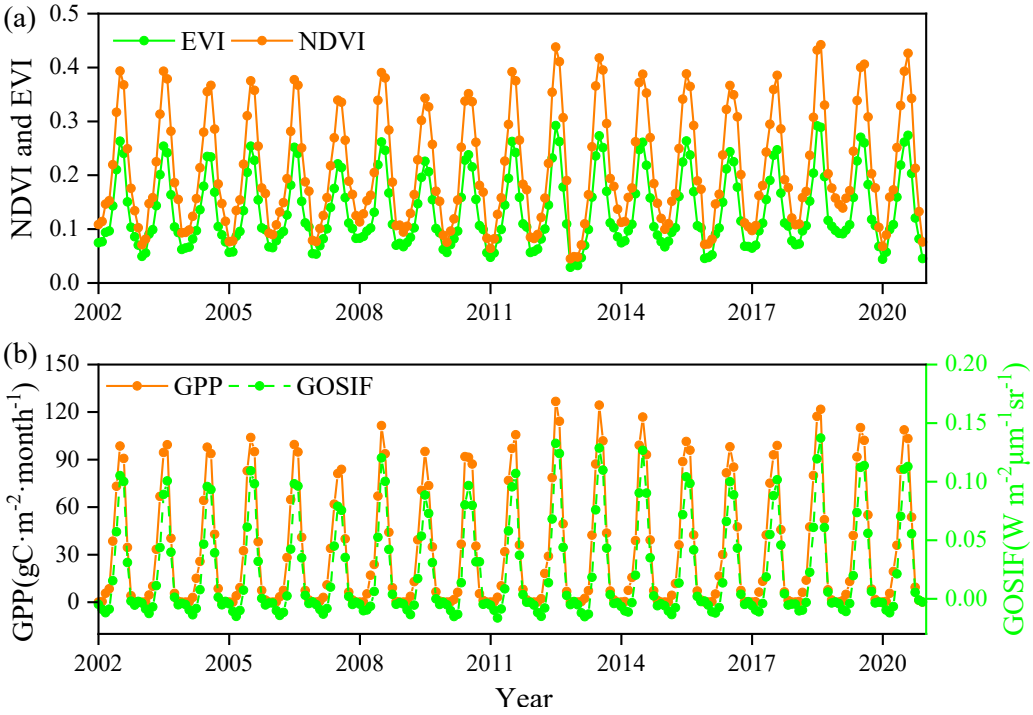

Figure 2. Temporal trends of monthly grassland (a) NDVI, EVI, (b) GOSIF, and GPP.

In Figure 3, the yearly trends of NDVI, EVI, GOSIF and GPP from 2000 to 2020 are depicted. All four variables exhibited significant increasing trends during this period, with change rates of 0.0024 a^{-1}, 0.0018 a^{-1}, 0.0012 $W \cdot m^{-2} \cdot \mu m^{-1} \cdot sr^{-1} \cdot a^{-1}$ and 4.6950 $gC \cdot m^{-2} \cdot a^{-1}$, respectively ($P$<0.01). The peak values for grassland NDVI, EVI, GOSIF and GPP were observed in 2018, reaching 0.4617, 0.3145, 0.1394 $W \cdot m^{-2} \cdot \mu m^{-1} \cdot sr^{-1}$ and 447.7892 $gC \cdot m^{-2}$, respectively. Conversely, the minimum lowest values for grassland NDVI and EVI were recorded in 2009 at 0.3593 and 0.2381 (Figure 3a), while the lowest values for grassland GOSIF and GPP were observed in 2007, with values of 0.0856 $W \cdot m^{-2} \cdot \mu m^{-1} \cdot sr^{-1} \cdot a^{-1}$ and 322.67 $gC \cdot m^{-2} \cdot a^{-1}$ (Figure 3b).

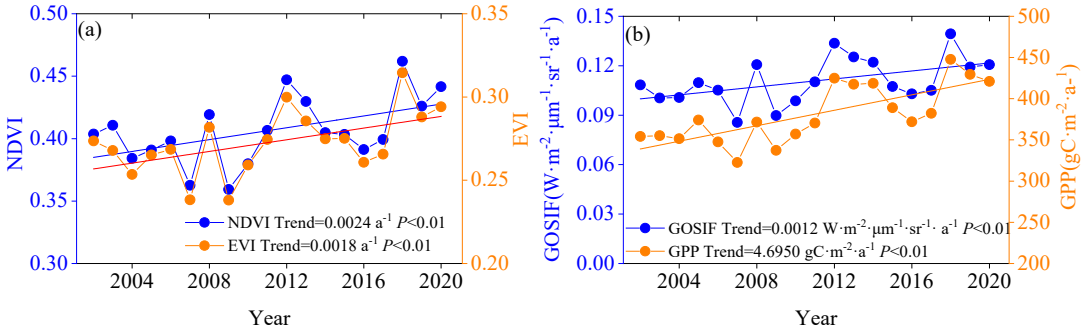

Figure 3. Temporal variations of annual (a) NDVI, EVI, (b) GOSIF, and GPP during 2002 to 2020

Figure 4 illustrates the spatial patterns and change trends of grassland NDVI, EVI, GOSIF, and GPP in Inner Mongolia between 2002 and 2020. The annual mean values of these variables showed similar spatial distribution characteristics, gradually increasing from the northwest to the southeast (Figure 4a-4d). High values were primarily concentrated in the eastern part of t Inner Mongolia, including LM and TMS regions (Figure 4a-4d and Figure 1), while lower values prevailed in the western orgions, which are predominantly TD and TSD (Figure 4a-4d and Figure 1). Spatial variability in grassland change trends across Inner Mongolia from 2002 to 2020 was evident. For NDVI and EVI, approximately 82.13% and 80.18% of the region displayed increasing trends. Notably, 25.83% and 21.18% of the grassland NDVI and EVI values showed significant increasing trends, primarily concentrated in Tongliao, Ordos and Alxa League (Figure 1 and Figure 4e-4f). Conversely, only 0.91%

Preprints (www.preprints.org) | NOT PEER-REVIEWED | Posted: 2 October 2023 doi:10.20944/preprints202310.0075.v1

and 0.82% of the grassland NDVI and EVI values exhibited significant decreasing trends, scattered in areas such as Chifeng and Alxa League (Figure 1 and Figure 4e-4f). As for grassland GOSIF and GPP, the areas showing increasing trends (84.42% and 96.89%) were substantially higher than those with decreasing trends (15.58% and 3.11%). Specifically, 22.65% and 48.13% of grassland GOSIF and GPP values showed significant increasing trends, primarily distributed in Xingan League, Tongliao, Chifeng, Ordos and Alxa League. These regions are mainly covered by TS, TSD, and TMS (Figure 1). Conversely, only 0.50% and 0.26% of the grassland GOSIF and GPP values showed significant decreasing trends in the study area.

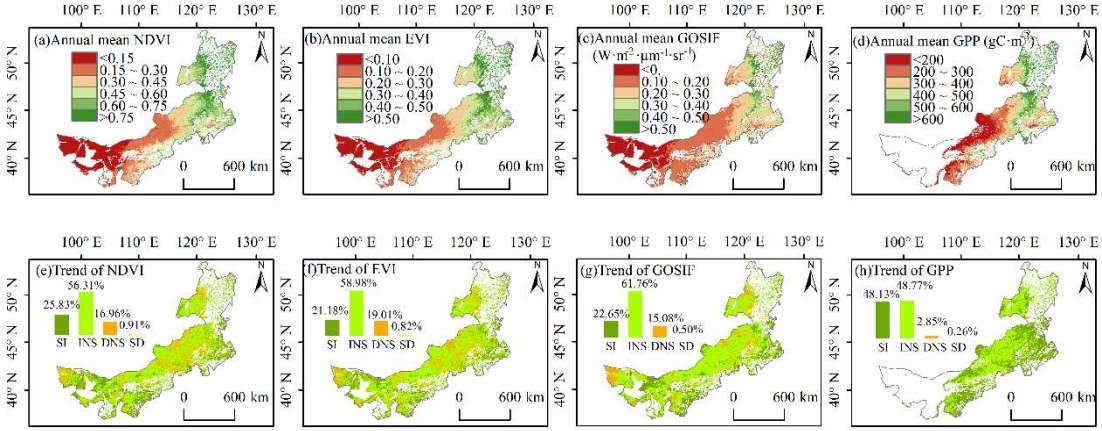

Figure 4. Spatial patterns and change trends of grassland NDVI, EVI, GOSIF, and GPP in Inner Mongolia between 2002 and 2020.

3.2. Changes of drought from 2002 to 2020

Figure 5 indicated the SPEI and standardized anomaly of CCI-SM ($SA_{CCI\text{-}SM}$) change trends from 2002 to 2020 in Inner Mongolia grassland. As shown in Figure 5, SPEI values exhibited frequent fluctuations at 1-month time (SPEI-1) or 3-month time (SPEI-3), while remaining relatively stable at longer time scales (SPEI-12). The pronounced amplitude and higher frequency of wet and dry changes were primarily associated with SPEI-1 (Figure 5a). From 2002 to 2020, Inner Mongolia grassland experienced a total of 96 drought months including 50 mild droughts, 33 moderate droughts, 12 severe droughts, and one extreme drought month. Among these, the lowest SPEI-1 value (-2.05) was recorded in March 2019 (Figure 5a). In contrast, SPEI-3 exhibited greater stability and provided insight into seasonal scale dry-wet changes. During the same period, a total of 119 drought months were recorded, comprising 54 mild droughts, 48 moderate droughts, 14 severe droughts, and 3 extreme droughts. The lowest SPEI-3 value (-2.08) occurred in June 2017 (Figure 5b). SPEI-12, reflecting the annual scale dry-wet variation, and was the most stable among the three indices. From 2002 to 2012, SPEI-12 identified 57 mild droughts, 71 moderate droughts, 23 severe droughts and 6 extreme droughts. The lowest SPEI-12 value (-2.11) was found in March 2018 (Figure 5c). In particular, SPEI-3 values were observed as -1.34, -1.45, -1.42, and -1.33 in June, July, August, and September 2007, respectively, and -2.08 and -2.0 in June and July 2017, respectively (Figure 5b).

The soil moisture status of Inner Mongolia grassland was identified by the $SA_{CCI\text{-}SM}$ (Figure 5d). From 2002 to 2020, a total of 112 drought months were identified by the soil moisture ($SA_{CCI\text{-}SM}<0$), with a minimum value of $SA_{CCI\text{-}SM}$ appearing in December 2020 ($SA_{CCI\text{-}SM}$ =-2.54). Notably, from June 2007 to September 2007, $SA_{CCI\text{-}SM}$ values consistently fell below -1 in Inner Mongolia grassland. Specifically, in June, July, August, September 2007, $SA_{CCI\text{-}SM}$ values were -1.59, -1.30, -1.71, and -1.91, respectively. In June and July 2017, $SA_{CCI\text{-}SM}$ values were -1.02 and -1.12, respectively (Figure 5d). Considering with the droughts indicated by SPEI-3 and $SA_{CCI\text{-}SM}$, June 2007 to September 2007 and June 2017 to July 2017 were selected to analyze the response of grassland vegetation growth to droughts.

Preprints (www.preprints.org) | NOT PEER-REVIEWED | Posted: 2 October 2023 doi:10.20944/preprints202310.0075.v1

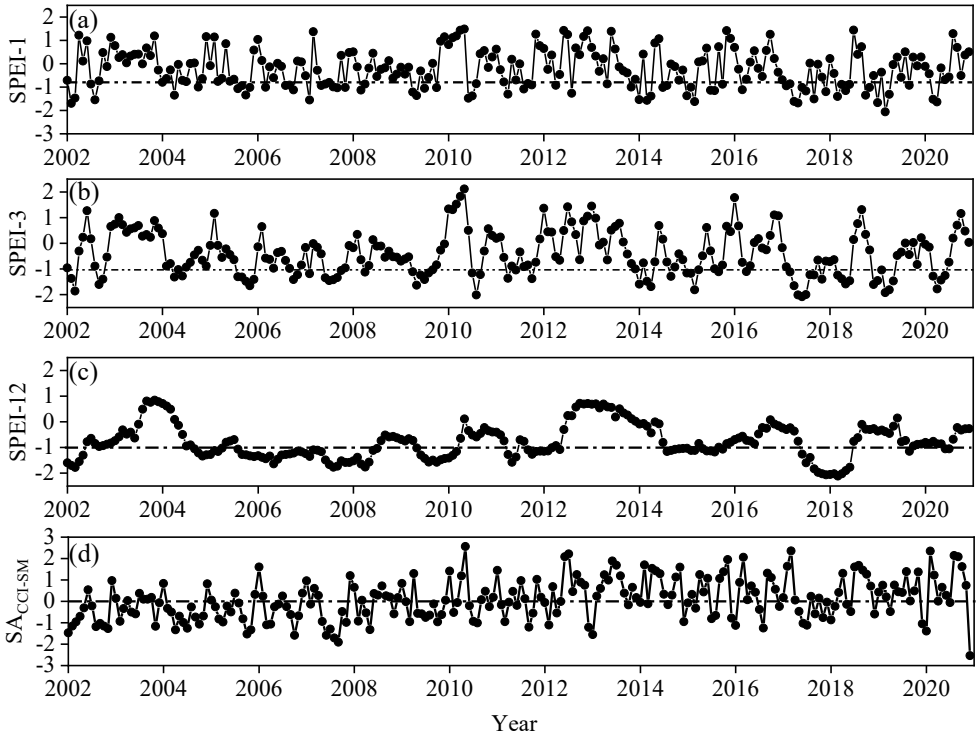

Figure 5. Temporal changes of SPEI and SA$_{CCI-SM}$, at monthly, seasonal, and annual scales.

Figure 6 and Figure 7 present the spatial patterns of SPEI-3 and SA$_{CCI-SM}$ in Inner Mongolia grassland for the years in 2007 and 2017. As illustrated in Figure 6, the percentage of grassland areas affected by severe and extreme drought was 47.98%, 59.24%, 63.01%, and 64.16%, respectively (Figure 6a-6d). These regions are primarily situated in the central eastern part of Inner Mongolia, with milder drought conditions observed in the western regions. The spatial distribution of SA$_{CCI-SM}$ closely mirrored that of SPEI-3. The proportion of areas with SA$_{CCI-SM}$ values less than -1 was 61.38%, 48.37%, 41.31% and 54.23%, respectively (Figure 6e-h). In June and July 2017, 61.27% and 56.36% of the grassland area showed extreme drought conditions, concentrated in the central eastern part of Inner Mongolia (Figure 7a and 7b). Spatial distribution of SA$_{CCI-SM}$ closely paralleled that of SPEI-3, with proportions of areas experiencing SA$_{CCI-SM}$ values less than -1 at 50.80% and 45.70%, respectively (Figure 7c and 7d).

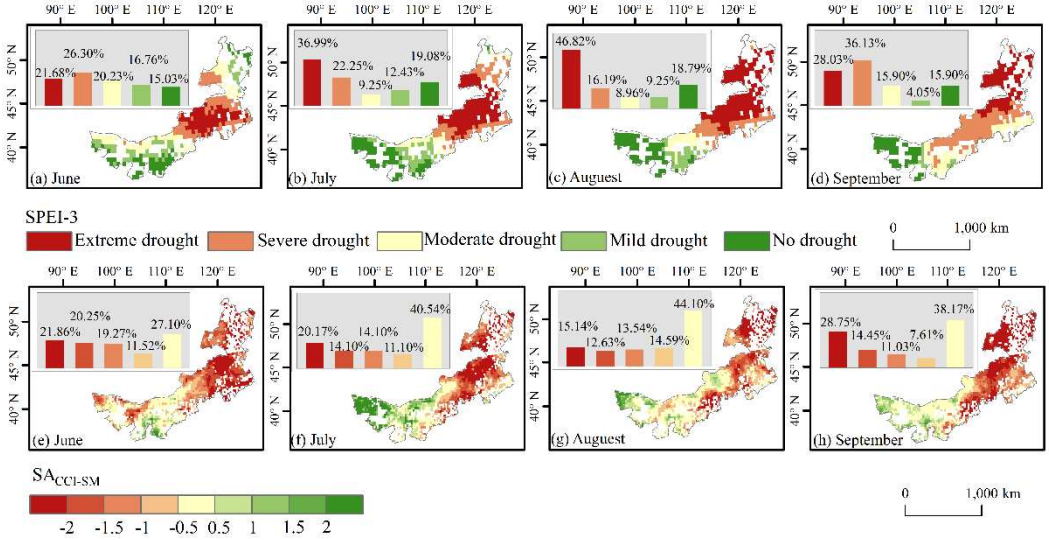

Figure 6. Spatial pattern of SPEI-3 and SA$_{CCI-SM}$ in June, July, Auguste, September 2007.

Preprints (www.preprints.org) | NOT PEER-REVIEWED | Posted: 2 October 2023 doi:10.20944/preprints202310.0075.v1

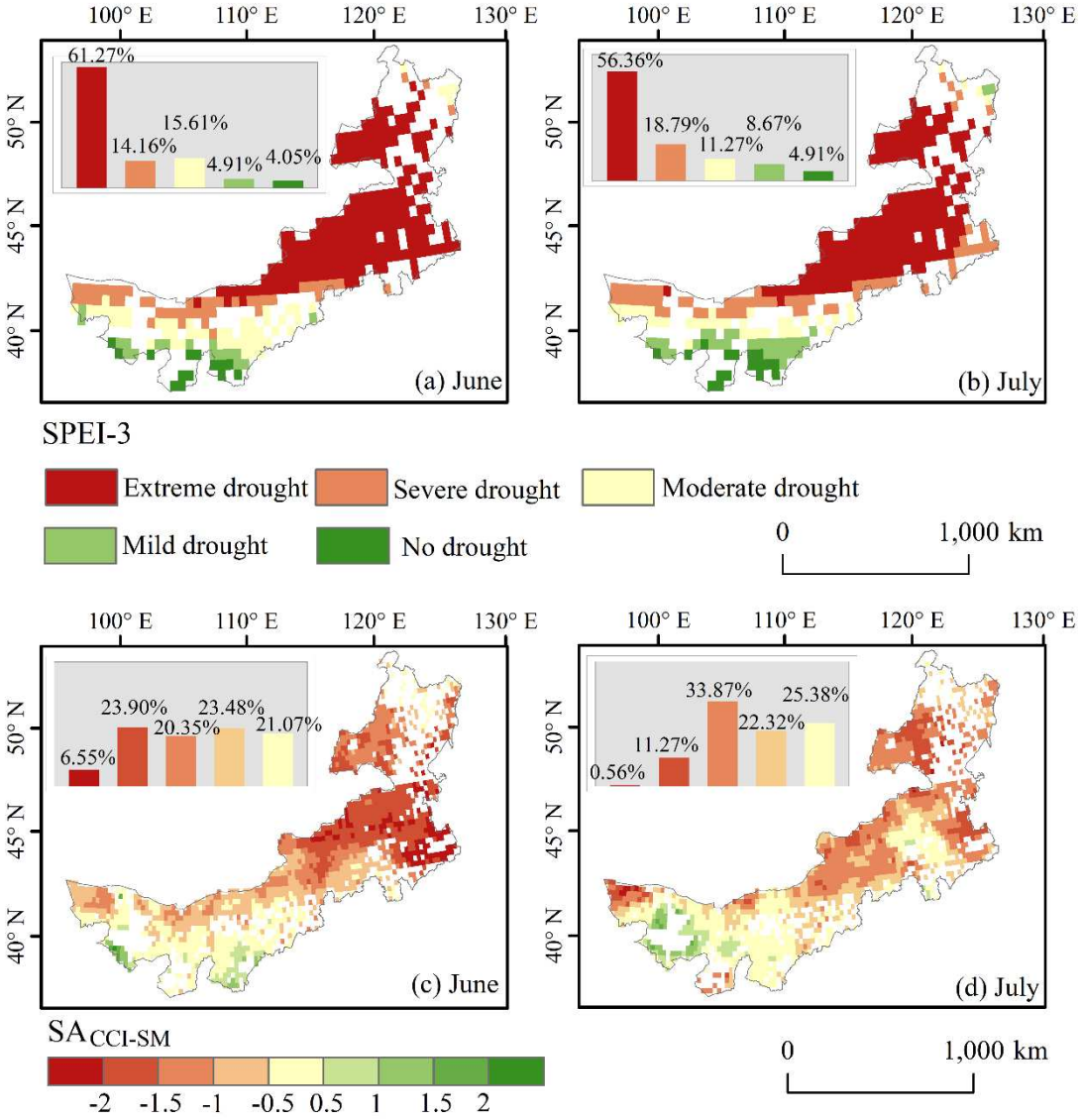

Figure 7. Spatial pattern of SPEI-3 and SA$_{CCI-SM}$ in June and July 2017.

3.3. Divergent grassland vegetation growth response to two drought events

Figure 8 and Figure 9 showed the spatial distributions of SA for NDVI, EVI, GOSIF and GPP during June, July, August, September 2007, as well as June and July 2017. Spatially, both NDVI and EVI indicated widespread declines (SA<-0.5) in during these months, particularly in east-central regions of Inner Mongolia (SA < -2) (Figure 8a-h). Specifically, NDVI decreased by 17.39%, 11.38%, 10.80% and 6.18% in June (-0.047), July (-0.039), August (-0.036) and September (-0.016), respectively, relative to the multi-year average (Figure 9a and 9b). Similarly, EVI declined by 18.33%, 13.97%, 11.24% and 4.98% in June, July, August, and September, confirming a widespread vegetation browning phenomenon following drought from June to September 2007. Compared to NDVI and EVI, GOSIF indicated a similar spatial distribution pattern but displayed more drastic changes from June to September (Figure 8i-l). GOSIF decreased by 34.37%, 30.42%, 29.88% and 14.12% in June (-0.015 Wm^{-2} μm^{-1} sr^{-1}), July (-0.024 Wm^{-2} μm^{-1} sr^{-1}), August (-0.023 Wm^{-2} μm^{-1} sr^{-1}), and September (-0.005 Wm^{-2} μm^{-1} sr^{-1}), respectively, relative to the multi-year average (2002-2020) (Figure 9e and 9f). The spatial distributions of SA for GPP indicated a net loss in carbon sequestration relative to the multi-year average becauseof the drought events. As a result, GPP decreased by 26.59%, 26.51%, 25.41%, and 10.28% in June (-10.93 gCm^{-2}), July (-17.58 gCm^{-2}), August (-16.23 gCm^{-2}), and September (-3.48 gCm^{-2}), respectively, relative to the multi-year average (2002-2020) (Figure 9g and 9h).

Preprints (www.preprints.org) | NOT PEER-REVIEWED | Posted: 2 October 2023 doi:10.20944/preprints202310.0075.v1

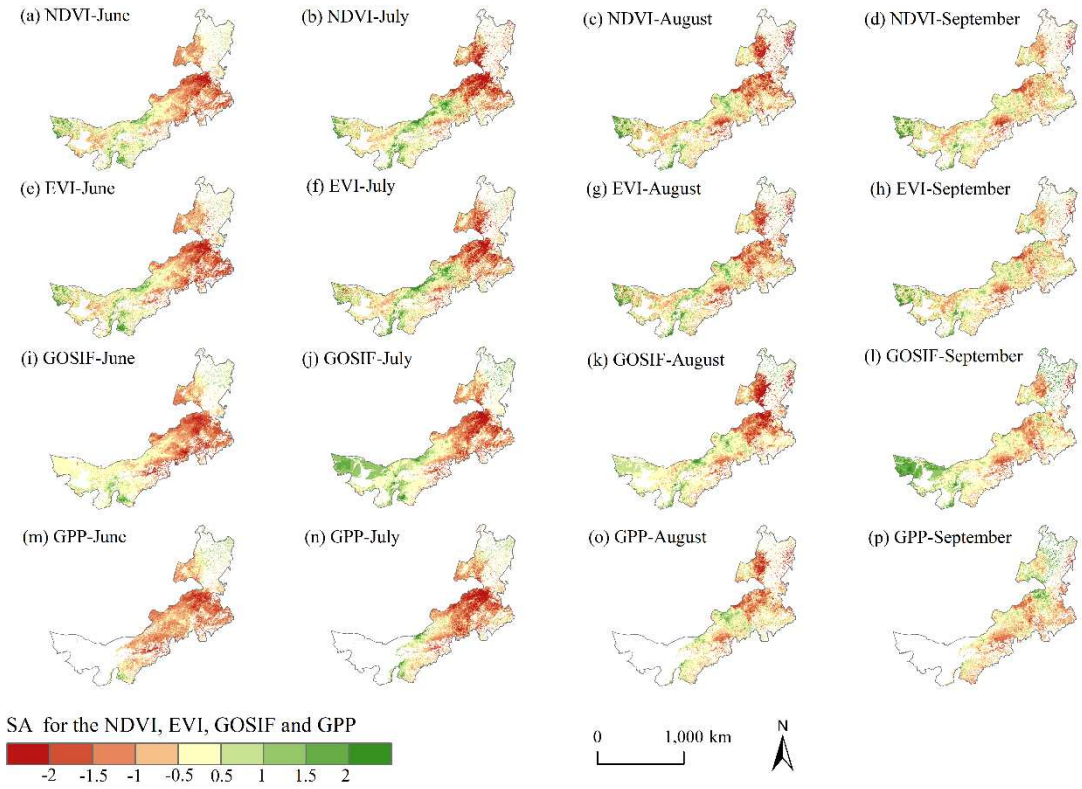

Figure 8. The spatial distributions of SA for NDVI, EVI, GOSIF, and GPP in June, July, August, September 2007.

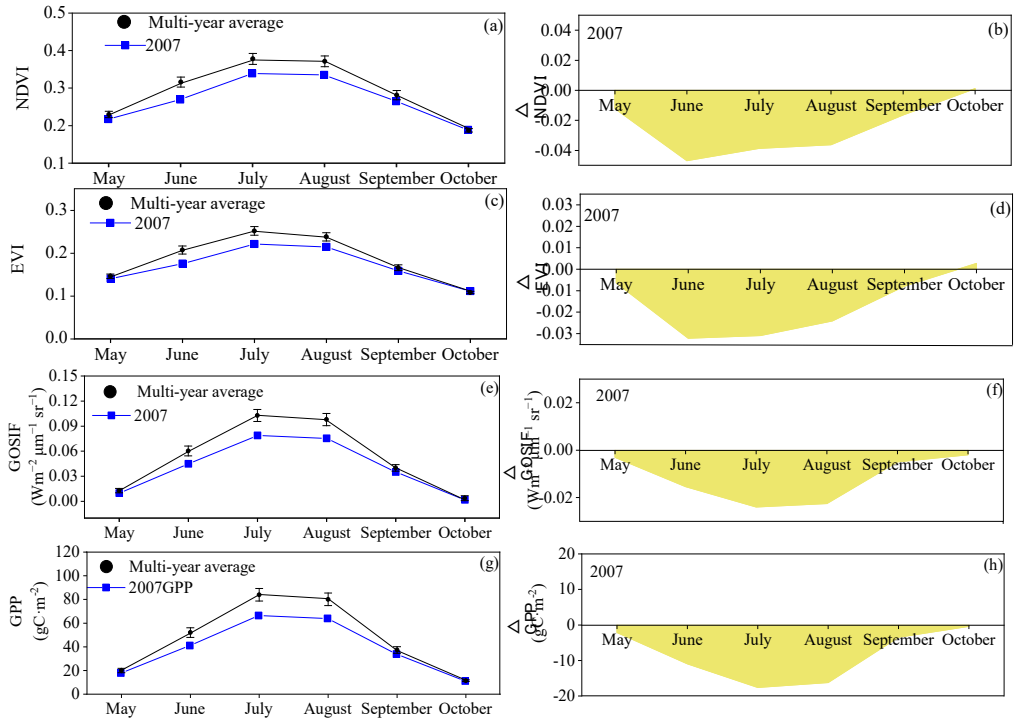

Figure 9. Temporal variation of NDVI, EVI, GOSIF, and GPP during the June, July, August, September drought in 2007

In June-July 2017, NDVI, EVI, GOSIF and GPP revealed a significant inhibition of grassland vegetation growth in east-central Inner Mongolia (SA < -0.5) (Figure 10). NDVI decreased by 7.31% and 5.22% in June (-0.022) and July (-0.019), respectively (Figure 11a and 11b). Similarly, EVI exhibited reductions of 9.05% and 6.36% in June (-0.017) and July (-0.015), respectively (Figure 11c and 11d).

Preprints (www.preprints.org) | NOT PEER-REVIEWED | Posted: 2 October 2023 doi:10.20944/preprints202310.0075.v1

Under the influence of drought stress, GOSIF decreased 10.20% and 17.01% in June (-0.006 Wm^{-2} μm^{-1} sr^{-1}) and July (-0.015 Wm^{-2} μm^{-1} sr^{-1}), respectively, signifying a clear inhibition of grassland vegetation growth (Figure 11e and 11f). GPP decreased by 8.33% and 14.91% in June (-4.001 gCm^{-2}) and July (-10.893 gCm^{-2}), respectively (Figure 11g and 11h). Notably, the decrease in GPP in June was less pronounced than in July. This differential response was particularly evident in GOSIF, while NDVI and EVI failed to capture this variability. Therefore, GOSIF emerges as a superior indicator for assessing the impact of drought events on grassland photosynthesis.

Based on the responses of NDVI, EVI, and GOSIF to two drought events, NDVI, EVI, and GOSIF experienced water stress during the peak growth stage of grassland vegetation. However, GOSIF exhibited a more pronounced response to drought, with its change trend closely mirroring that of GPP. Therefore, GOSIF serves as a valuable indicator that closely reflects the processes associated with GPP during drought events.

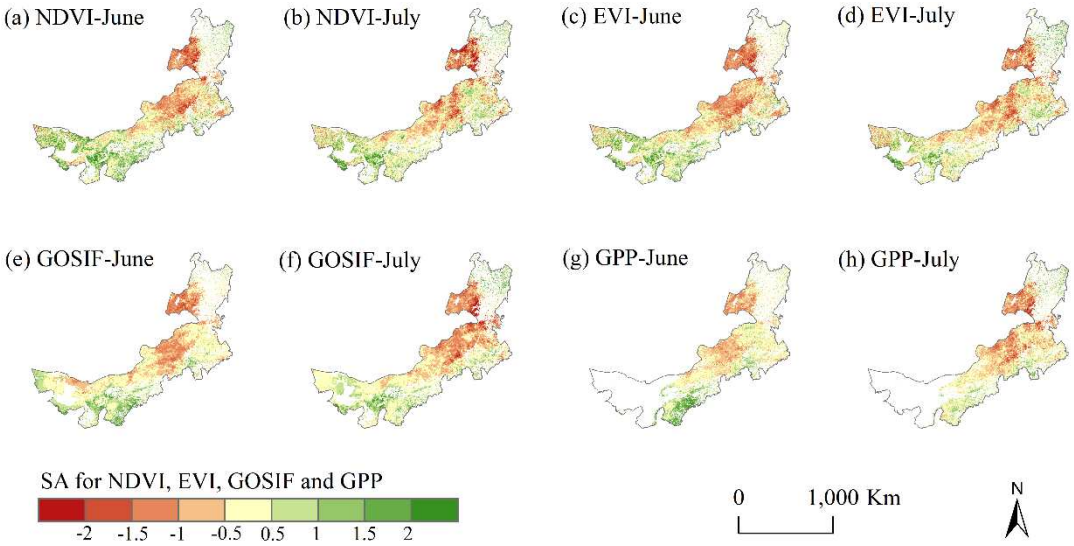

Figure 10. The spatial distributions of SA for NDVI, EVI, GOSIF, and GPP in June and July 2017.

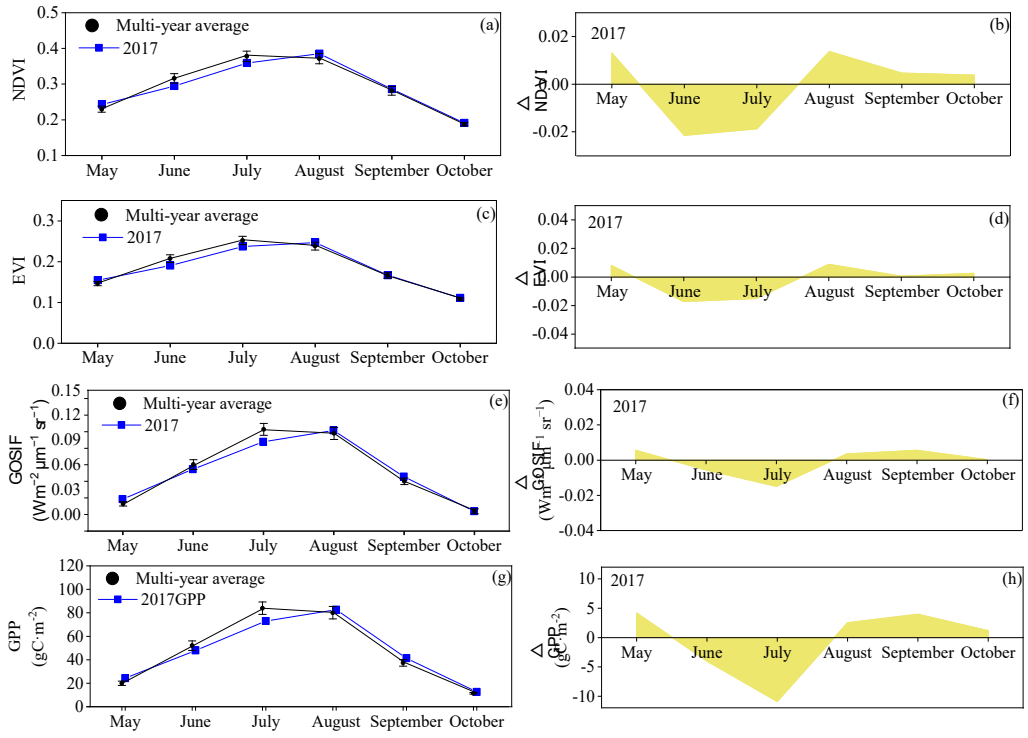

Figure 11. Temporal variation of NDVI, EVI, GOSIF, and GPP during the July and August drought in 2017.

Preprints (www.preprints.org) | NOT PEER-REVIEWED | Posted: 2 October 2023 doi:10.20944/preprints202310.0075.v1

3.4. NDVI, EVI, GOSIF and GPP loss in different drought-levels

In order to evaluate the impacts of different drought severities levels events in grassland vegetation, we examined the NDVI, EVI, GOSIF, and GPP reductions across varying drought severities in Inner Mongolia. In general, all levels of drought (moderate, severe, and extreme) led to the declines in NDVI, EVI, GOSIF, and GPP (Table 2). However, the extent of NDVI, EVI, GOSIF, and GPP reductions varied significantly. For NDVI, the average reductions caused by moderate, severe, and extreme droughts were 8.82%, 14.46% and 26.81%, respectively. Similarly, EVI exhibited average reductions of 8.71%, 15.04% and 27.11% under moderate, severe, and extreme droughts conditions, respectively. Notably, GOSIF showed much larger reductions in grassland of the Inner Mongolia, with reductions of 20.58%, 22.83% and 67.31% under moderate, severe, and extreme droughts, respectively. For GPP, the average reductions caused by moderate, severe, and extreme droughts was 10.52%, 18.01% and 27.05%, respectively. Overall, NDVI, EVI, GOSIF, and GPP exhibited decreased significant declines with increasing drought severity, with GOSIF displaying the most pronounced response to drought.

Table 2. The NDVI, EVI, GOSIF, and GPP reductions along the different drought levels in Inner Mongolia grassland.

	Moderate drought	**Severe drought**	**Extreme drought**
NDVI	8.82%	14.46%	26.81%
EVI	8.71%	15.04%	27.11%
GOSIF	20.58%	22.83%	67.31%
GPP	10.52%	18.01%	27.05%

The reductions in NDVI, EVI, GOSIF, and GPP across various grassland types along the drought severity gradient exhibit notable differences (Figure 12). During extreme drought conditions, the most significant NDVI reductions were observed in TS, with an average loss of -31.54%. LM, TMS, and TSD was also experienced substantial NDVI reductions, with average-16.88%, -16.52%, and -27.37% (Figure 12a). A similar pattern was observed for EVI reductions, where TS, LM, TMS, and TSD exhibited reductions of -31.69%, -17.25%, -20.45%, and -25.30%, respectively (Figure 12b). Remarkably, GOSIF reductions were most pronounced in TS, with an average loss of -92.15%, followed by LM (-67.72%), TSD (-61.37%), and TMS (-36.08%) (Figure 12c). Regarding GPP, TS experienced the highest average loss (-32.29%), followed by TSD (-23.73%), TMS (-20.28%), and LM (-19.01%) (Figure 12d). For severe drought conditions, GOSIF reductions in TS, LM, TMS, and TSD were -65.83%, -53.23%, -33.96%, and -53.94%, respectively (Figure 12c). GPP exhibited average losses of -23.42%, -15.40%, -15.28%, and -16.87%, in TS, LM, TMS, and TSD, respectively (Figure 12d). These findings highlight the significant variation in NDVI, EVI, GOSIF and GPP reductions across different grassland types within the context of the same level of drought. TS displayed the most substantial decrease ratio, while TMS exhibited the smallest decrease ratio.

Preprints (www.preprints.org) | NOT PEER-REVIEWED | Posted: 2 October 2023 doi:10.20944/preprints202310.0075.v1

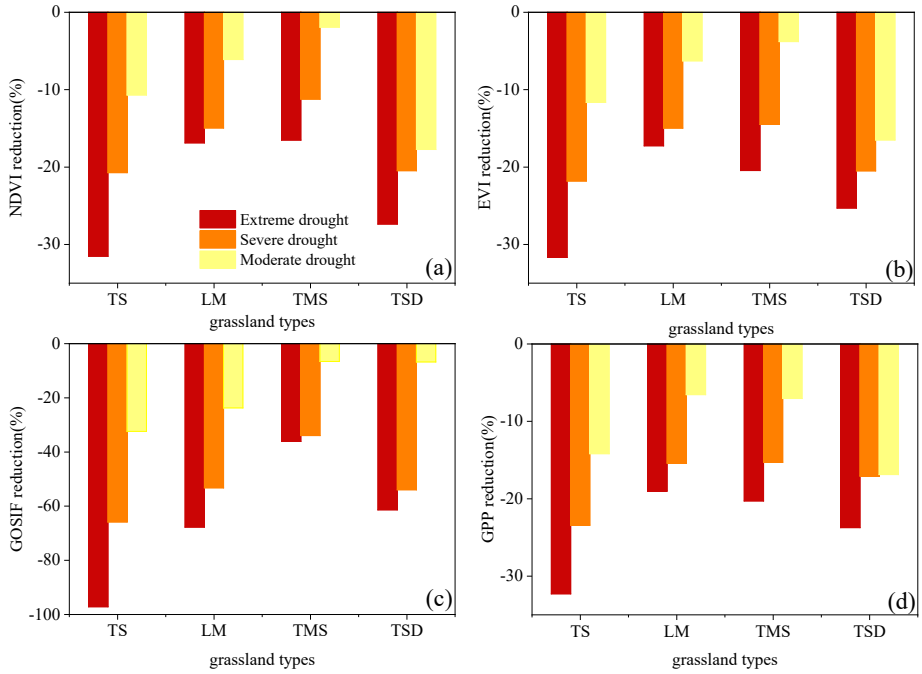

Figure 12. NDVI, EVI, GOSIF and GPP reductions (%) in different grassland types along the drought severity gradient.

4. Discussion

4.1. NDVI, EVI, GOSIF and GPP loss in different drought-levels

In this study, an overall decrease of grassland vegetation growth during the 2007 and 2017 drought events was found in Inner Mongolia (Figure 8 and Figure 10). This finding aligns with similar observations in other regions, such as southwest or northern China, U.S. Midwest, the tropical Amazon and temperate Europe [2,53,54]. Moreover, we found that the decrease in grassland GOSIF was much more substantial than that observed in NDVI and EVI during 2007 and 2017 drought events (Figure 9 and Figure 11). This heightened sensitivity of GOSIF to drought event in Inner Mongolia's grassland is significant. SIF captures information about vegetation photosynthesis, such as Absorbed Photosynthetically Active Radiation (FPAR) and light use efficiency [55]. As a sensitive indicator of vegetation photosynthesis, SIF can more realistically and sensitively reflect variations in canopy photosynthesis compared to traditional vegetation indices [18]. For example, studies conducted in the U.S. Midwest and Hulun Buir grassland have demonstrated that GOSIF is more sensitive to drought than NDVI and EVI [19,54]. Previous studies have also highlighted the superior performance of SIF is capturing variations in GPP during drought events [36,54]. Our findings further support the viewpoint which the trend in GPP closely aligns with that of GOSIF during 2007 and 2017 drought events (Figure 9 and Figure 11).

4.2. NDVI, EVI, GOSIF and GPP response under different drought severities

This study also quantified the grassland NDVI, EVI, GOSIF and GPP loss under different drought severity levels, and reductions variation in different grassland types within the context of the same drought level, which is critical for identifying grassland most sensitive to severe and extreme drought events (Table 2 and Figure 12). Our finding confirmed that NDVI, EVI, GOSIF and GPP all exhibited substantial decrease as drought severity increased, aligning with previous researches [10,24]. For different grassland types, TS ecosystems were the most vulnerable to severe and extreme droughts in Inner Mongolia. TS regions, primarily studied in the semi-arid region of central Inner Mongolia (Figure 1b), displayed the highest reduction rates. This heightened vulnerability can be attributed to the unique characteristics of semi-arid ecosystems, which tend to exhibit the most pronounced physiological and functional responses to drought stress [24,56,57]. These findings align with similar observations in other semi-arid regions, such as southeastern Australia.

The TSD ecosystems exhibited the second-largest reduction in response to drought. TSD regions are mostly found in the arid western part of Inner Mongolia (Figure 1). While TSD ecosystems have adapted to living in arid conditions, extreme or severe droughts can still have detrimental effects. These conditions can lead to structural changes and reduced photosynthesis, as observed in our study and supported by previous research [24,56].

4.3. Uncertainties

While this study provides valuable insights NDVI, EVI, GOSIF, and GPP trends and their responses to droughts in Inner Mongolia grassland, several limitations should be considered. Firstly, although GOSIF dataset, while offering continuity in spatiotemporal distribution, features relatively coarse resolution (0.05°×0.05°). Additionally, GOSIF is derived from a machine learning method based on OCO-2 satellite data, which introduces certain internal uncertainties [22,32]. Secondly, previous studies found the grasslands in Inner Mongolia may experience by compound droughts [58]. This study focused on the response to individual drought events, and further research should investigate how grassland vegetation responds to these more complex and compounded drought scenarios. Moreover, this study assessed the impact of SPEI on grassland vegetation. The vapor pressure deficit (VPD), soil moisture and human activities can also affect vegetation growth [59,61], and ignoring these variables will inevitably result in some uncertainties of the presented results. Therefore, these questions will need to be discussed and analyzed in future studies.

5. Conclusions

In this study, we utilized NDVI, EVI, GOSIF, GPP, and drought indices to assess the effect of drought events on grassland ecosystems in Inner Mongolia of China. Our investigation aimed to uncover spatiotemporal evolution patterns of grassland dynamics and evaluate how different drought severity levels affect various grassland types. This study shows that NDVI, EVI, GOSIF, and GPP exhibited significant increasing trends from 2000 to 2020, with 25.83%, 21.18%, 22.65% and 48.13% of the grassland areas, respectively. Compared with NDVI and EVI, the responses of GOSIF to drought more intense, and it can better reflect the impact of drought events on grassland photosynthesis in 2007 and 2017. The reductions in NDVI, EVI, GOSIF, and GPP intensified as drought severity levels increased. The influence of drought events on NDVI, EVI, GOSIF, and GPP reductions in different grassland types under extreme drought conditions was obviously different, and the effects of different drought-levels in same grassland type were also exist difference. These findings underscore the critical importance of effectively managing land carbon cycling and addressing the challenges posed by climate change, particularly in regions like Inner Mongolia, where grassland ecosystems play a vital role.

6. Patents

Acknowledgments: This study was financially supported by the National Key Research and Development Program of China (No.2021YFB3901201), the National Natural Science Foundation of Hebei Province, China (No. D2022402030).

Declaration of Competing Interest: All authors declare that No conflict of interest exists.

Author Contributions: "Conceptualization, A.Zhao. and X.Zhu.; methodology, A.Zhao.; software, R.Xu.; validation, A.Zhao.; R.Xu. and L.Zou.; formal analysis, R.Xu.; investigation, R.Xu.; resources, X.Zhu.; data curation, A.Zhao.; writing—original draft preparation, L.Zou.; writing—review and editing, A.Zhao.; visualization, A.Zhao.; supervision, A.Zhao.; project administration, X.Zhu.; funding acquisition, Y.Y. All authors have read and agreed to the published version of the manuscript."

Funding: Please add: "This research received no external funding" or "This research was funded by he National Key Research and Development Program of China, grant number 2021YFB3901201" and "National Natural Science Foundation of Hebei Province, China, grant number D2022402030.

References

1. Heim. R. R.; A review of twentieth-century drought indices used in the United States. Bull. Am. Meteorol. Soc. 2002, 83, 1149-1166. https://doi.org/10.1175/1520-0477-83.8.1149.

2. Li, X.; Li, Y.; Chen, A.; Gao, M.; Slette, I. J.; Piao, S.; The impact of the 2009/2010 drought on vegetation growth and terrestrial carbon balance in Southwest China. Agr. Forest. Meteorol. 2019, 269, 239-248. https://doi.org/10.1016/j.agrformet.2019.01.036.
3. West, H.; Quinn, N.; Horswell, M.; Remote sensing for drought monitoring & impact assessment: Progress, past challenges and future opportunities. Remote. Sens. Environ. 2019, 232, 111291. https://doi.org/10.1016/j.rse.2019.111291.
4. AghaKouchak, A.; Huning, L. S.; Sadegh, M.; Qin, Y.; Markonis, Y.; Vahedifard, F.; Love, C. A.; Mishra, A.; Mehran, A.; Obringer, R.; Hjelmstad, A.; Pallickara, S.; Jiwa, S.; Hanel, Martin.; Zhao, Y.; Pendergrass, A. G.; Arabi, M.; Davis, S. J.; Ward, P.J.; Svoboda, M.; Pulwarty, R.; Kreibich, H.; Toward impact-based monitoring of drought and its cascading hazards. Nat. Rev. Earth. Env. 2023, 4, 582-595. https://doi.org/10.1038/s43017-023-00457-2.
5. Bennett, A. C.; McDowell, N. G.; Allen, C. D.; Anderson-Teixeira, K. J.; Larger trees suffer most during drought in forests worldwide. Nat. Plants. 2015, 1, 15139. https://doi.org/10.1038/nplants.2015.139.
6. Feng, W.; Lu, H.; Yao, T.; Yu, Q.; Drought characteristics and its elevation dependence in the Qinghai–Tibet plateau during the last half-century. Sci. Rep-UK, 2020, 10, 14323. https://doi.org/10.1038/s41598-020-71295-1.
7. Liu, Y.; Dang, C.; Yue, H.; Lyu, C.; Dang, X.; Enhanced drought detection and monitoring using sun-induced chlorophyll fluorescence over Hulun Buir Grassland, China. Sci. Total. Environ. 2021, 770, 145271. https://doi.org/10.1016/j.scitotenv.2021.145271.
8. Vicente-Serrano, S. M.; Quiring, S. M.; Pena-Gallardo, M.; Yuan, S.; Dominguez-Castro, F.; A review of environmental droughts: Increased risk under global warming?. Earth-Sci. Rev. 2020, 201, 102953. https://doi.org/10.1016/j.earscirev.2019.102953.
9. Cao, D.; Zhang, J.; Han, J.; Zhang, T.; Yang, S.; Wang, J.; Prodhan, F. A.; Yao, F.; Projected increases in global terrestrial net primary productivity loss caused by drought under climate change. Earths. Future. 2022, 10, e2022EF002681. https://doi.org/10.1029/2022EF002681.
10. Lei, T.; Feng, J.; Lv, J.; Wang, J.; Song, H.; Song, W.; Gao, X.; Net Primary Productivity Loss under different drought levels in different grassland ecosystems. J. Environ. Manage. 2020, 274, 111144. https://doi.org/10.1016/j.jenvman.2020.111144.
11. Wang, X.; Pan, S.; Pan, N.; Pan, P.; Grassland productivity response to droughts in northern China monitored by satellite-based solar-induced chlorophyll fluorescence. Sci. Total. Environ. 2022, 830, 154550. https://doi.org/10.1016/j.scitotenv.2022.154550.
12. Deng, L.; Shangguan, Z.; Bell, S. M.; Soromotin, A. V.; Peng, C.; An, S.; Wu, X.; Xu, X.; Wang, K.; Li, J.; Tang, Z.; Yan, W.; Zhang, F.; Li, J.;Wu, J.; Kuzyakov, Y.; Carbon in Chinese grasslands: meta-analysis and theory of grazing effects. Carbon. Res. 2023, 2,19. https://doi.org/10.1007/s44246-023-00051-7.
13. Sun, J.; Liu, W.; Pan, Q.; Zhang, B.; Lv, Y.; Huang, J.; Han, X.; Positive legacies of severe droughts in the Inner Mongolia grassland. Sci. Adv. 2022, 8, eadd6249. https://doi.org/10.1126/sciadv.add6249.
14. AghaKouchak, A.; Farahmand, A.; Melton, F. S.; Teixeira, J.; Anderson, M. C.; Wardlow, B. D.; Hain, C. R.; Remote sensing of drought: Progress, challenges and opportunities. Rev. Geophys. 2015, 53(2), 452-480. https://doi.org/10.1002/2014RG000456.
15. Jiao, W.; Wang, L.; McCabe, M. F.; Multi-sensor remote sensing for drought characterization: current status, opportunities and a roadmap for the future. Remote. Sens. Environ. 2021, 256, 112313. https://doi.org/10.1016/j.rse.2021.112313.
16. Jiao, W.; Wang, L.; Smith, W. K.; Chang, Q.; Wang, H.; D'Odorico, P.; Observed increasing water constraint on vegetation growth over the last three decades. Nat. Commun. 2021, 12, 3777. https://doi.org/10.1038/s41467-021-24016-9.
17. Meroni, M.; Rossini, M.; Guanter, L.; Alonso, L.; Rascher, U.; Colombo, R.; Moreno, J.; Remote. sensing of solar-induced chlorophyll fluorescence: Review of methods and applications. Remote. Sens. Environ. 2009, 113, 2037-2051. https://doi.org/10.1016/j.rse.2009.05.003.
18. Xu, H. J.; Wang, X. P.; Zhao, C. Y.; Drought sensitivity of vegetation photosynthesis along the aridity gradient in northern China. Int. J. Appl. Earth. Obs. 2021, 102, 102418. https://doi.org/10.1016/j.jag.2021.102418.
19. Liu, Y.; You, C.; Zhang, Y.; Chen, S.; Zhang, Z.; Li, J.; Wu, Y.; Resistance and resilience of grasslands to drought detected by SIF in inner Mongolia, China. Agr. Forest. Meteorol. 2021, 308-309, 108567. https://doi.org/10.1016/j.agrformet.2021.108567.
20. Zhao, A.; Wang, D.; Xiang, K.; Zhang, A.; Vegetation photosynthesis changes and response to water constraints in the Yangtze River and Yellow River Basin, China. Ecol. Indic. 2022, 143, 109331. https://doi.org/10.1016/j.ecolind.2022.109331.
21. Mohammed, G. H.; Colombo, R.; Middleton, E. M.; Rascher, U.; van der Tol, C.; Nedbal, L.; Goulas, Y.; Pérez-Priego, O.; Damm, A.; Meroni, M.; Joanna, J.; Cogliati, S.; Verhoef, W.; Malenovský, Z.; Gastellu-Etchegorry, J. P.; Miller, J. R.; Guanter, L.; Moreno, J.; Moya, I.; Berry, J. A.; Frankenberg, C.; Zarco-Tejada, P. J.; Remote sensing of solar-induced chlorophyll fluorescence (SIF) in vegetation: 50 years of progress. Remote. Sens. Environ. 2019, 231, 111177. https://doi.org/10.1016/j.rse.2019.04.030.

22. Zhang, T.; Zhou, J.; Yu, P.; Li, J.; Kang, Y.; Zhang, B. Response of ecosystem gross primary productivity to drought in northern China based on multi-source remote sensing data. J. Hydrol. 2023, 616, 128808. https://doi.org/10.1016/j.jhydrol.2022.128808.
23. Wang, Q.; Zeng, J.; Qi, J.; Zhang, X.; Zeng, Y.; Shui, W.; Xu, Z.; Zhang, R.; Wu, X.; Cong, J.; A multi-scale daily SPEI dataset for drought characterization at observation stations over mainland China from 1961 to 2018. Earth. Syst. Sci. Data. 2021, 13, 331-341. https://doi.org/10.5194/essd-13-331-2021.
24. Wang, S.; Li, R.; Wu, Y.; Zhao, S.; Vegetation dynamics and their response to hydrothermal conditions in Inner Mongolia, China. Glob. Ecol. Conserv. 2022, 34, e02034. https://doi.org/10.1016/j.gecco.2022.e02034.
25. Tong, S.; Bao, G.; Bao, Y.; Huang, X.; Monitoring of long-term vegetation dynamics and responses to droughts of various timescales in Inner Mongolia. Ecosphere. 2023, 14, e4415. https://doi.org/10.1002/ecs2.4415.
26. Tong, S.; Zhang, J.; Bao, Y.; Inter-decadal spatiotemporal variations of aridity based on temperature and precipitation in Inner Mongolia, China. Pol. J. Environ. Stud. 2017, 26, 819-826. https://doi.org/10.15244/pjoes/65840.
27. Bian, Y.; Dai, H.; Zhang, Q.; Yang, L.; Du, W.; Spatial distribution of potential evapotranspiration trends in the Inner Mongolia Autonomous Region (1971–2016). Theor. Appl. Climatol. 2020, 140, 1161-1169. https://doi.org/10.1007/s00704-020-03154-y.
28. Chen, X.; Peng, J.; Li, H.; Seasonal and regional differences of air temperature changes in Inner Mongolia. Geogr. Res. 2009, 28, 27-35.
29. Cai, S.; Song, X.; Hu, R.; Leng, P.; Li, X.; Guo, D.; Zhang, Y.; Hao,Y.; Wang, Y.; Spatiotemporal characteristics of agricultural droughts based on soil moisture data in Inner Mongolia from 1981 to 2019. J. Hydrol. 2021, 603, 127104. https://doi.org/10.1016/j.jhydrol.2021.127104.
30. Holben, B. N.; Characteristics of maximum-value composite images from temporal AVHRR data. Int. J. Remote. Sens. 1986, 7, 1417-1434. https://doi.org/10.1080/01431168608948945.
31. Li, M.; Chu, R.; Sha, X.; Xie, P.; Ni, F.; Wang, C.; Jiang, Y.; Shen, S.; Islam, A. R. M. T.; Monitoring 2019 Drought and Assessing Its Effects on Vegetation Using Solar-Induced Chlorophyll Fluorescence and Vegetation Indexes in the Middle and Lower Reaches of Yangtze River, China. Remote. Sens-basel. 2022, 14, 2569. https://doi.org/10.3390/rs14112569.
32. Li, X.; Xiao, J.; A global, 0.05-degree product of solar-induced chlorophyll fluorescence derived from OCO-2, MODIS, and reanalysis data. Remote. Sens-basel. 2019, 11, 517. https://doi.org/10.3390/rs11050517.
33. Mohammadi, K.; Jiang, Y.; Wang, G.; Flash drought early warning based on the trajectory of solar-induced chlorophyll fluorescence. P. Natl. A. Sci. 2022, 119, e2202767119. https://doi.org/10.1073/pnas.2202767119
34. Yao, T.; Liu, S.; Hu, S.; Mo, X.; Response of vegetation ecosystems to flash drought with solar-induced chlorophyll fluorescence over the Hai River Basin, China during 2001–2019. J. Environ. Manage. 2022, 313, 114947. https://doi.org/10.1016/j.jenvman.2022.114947.
35. Vicente-Serrano, S. M.; Beguería, S.; López-Moreno, J. I.; A multiscalar drought index sensitive to global warming: the standardized precipitation evapotranspiration index. J. Climate. 2010, 23, 1696-1718. https://doi.org/10.1175/2009JCLI2909.1.
36. Zhang, R.; Bento, V. A.; Qi, J.; Xu, F.; Wu, J.; Qiu, J.; Li, J.; Shui, W.; Wang, Q.; The first high spatial resolution multi-scale daily SPI and SPEI raster dataset for drought monitoring and evaluating over China from 1979 to 2018. Big. Earth. Data. 2023, 1-26. https://doi.org/10.1080/20964471.2022.2148331.
37. Mohammed, S.; Alsafadi, K.; Enaruvbe, G. O.; Bashir, B.; Elbeltagi, A.; Széles, A.; Alsalman, A.; Harsanyi, E.; Assessing the impacts of agricultural drought (SPI/SPEI) on maize and wheat yields across Hungary. Sci. Rep-UK. 2022, 12, 8838. https://doi.org/10.1038/s41598-022-12799-w.
38. Musei, S. K.; Nyaga, J. M.; & Dubow, A. Z.; SPEI-based spatial and temporal evaluation of drought in Somalia. J. Arid. Environ. 2021, 184, 104296. https://doi.org/10.1016/j.jaridenv.2020.104296.
39. Zuo, D.; Cai, S.; Xu, Z.; Peng, D.; Kan, G.; Sun, W.; Pang, B.; Yang, H. Assessment of meteorological and agricultural droughts using in-situ observations and remote sensing data. Agr. Water. Manage. 2019, 222, 125-138. https://doi.org/10.1016/j.agwat.2019.05.046.
40. Dorigo, W.; Wagner, W.; Albergel, C.; Albrecht, F.; Balsamo, G.; Brocca, L.; Chung, D.; Ertl, M.; Forkel, M.; Gruber, A.; Haas, E.; Hamer, P. D.; Hirschi, M.; Ikonen, J.; de Jeu, R.; Kidd, R.; Lahoz, W.; Liu, Y. Y.; Miralles, D.; Mistelbauer, T.; Nicolai-Shaw, N.; Parinussa, R.; Pratola, C.; Reimer, C.; van der Schalie, R.; Seneviratne, S. I.; Smolander, T.; Lecomte, P.; ESA CCI Soil Moisture for improved Earth system understanding: State-of-the art and future directions, Remote. Sens. Environ. 2017, 203, 185-215. https://doi.org/10.1016/j.rse.2017.07.001.
41. Liu, K.; Li, X.; Wang, S.; Zhang, H.; A robust gap-filling approach for European Space Agency Climate Change Initiative (ESA CCI) soil moisture integrating satellite observations, model-driven knowledge, and spatiotemporal machine learning. Hydrol. Earth Syst. Sci. 2023, 27, 577-598. https://doi.org/10.5194/hess-27-577-2023.

42. González-Zamora, Á.; Sánchez, N.; Pablos, M.; A. M. U.; Martínez-Fernández, J.; CCI soil moisture assessment with SMOS soil moisture and in situ data under different environmental conditions and spatial scales in Spain. Remote. Sens. Environ. 2019, 225, 469-482. https://doi.org/10.1016/j.rse.2018.02.010.
43. Zhang, L.; Liu, Y.; Ren, L.; Jiang, S.; Yang, X.; Yuan, F.; Wang, M.; Wei, L.; Drought monitoring and evaluation by ESA CCI soil moisture products over the Yellow River Basin. IEEE. J-Stars. 2019, 12, 3376-3386. https://doi.org/10.1109/JSTARS.2019.2934732.
44. Ling, X.; Huang, Y.; Guo, W.; Wang, Y.; Chen, C.; Qiu, B.; Ge, J.; Qin, K.; Xue, Y.; Peng, J.; Comprehensive evaluation of satellite-based and reanalysis soil moisture products using in situ observations over China. Hydrol. Earth Syst. Sci. 2021, 25, 4209-4229. https://doi.org/10.5194/hess-25-4209-2021.
45. Trabucco, A.; R. J. Zomer.; 2009, Global aridity index (global-aridity) and global potential evapotranspiration (global-PET) geospatial database, CGIAR Consortium for Spatial Information.
46. Sun, Z.; Long, D.; Yang, W.; Li, X.; Pan, Y.; Reconstruction of GRACE data on changes in total water storage over the global land surface and 60 basins. Water. Resour. Res. 2020, 55, e2019WR026250. https://doi.org/10.1029/2019WR026250.
47. Li, S.; Xie, Y.; Brown, D. G.; Bai, Y.; Hua, J.; Judd, K.; Spatial variability of the adaptation of grassland vegetation to climatic change in Inner Mongolia of China. Appl. Geogr. 2013, 43, 1-12. https://doi.org/10.1016/j.apgeog.2013.05.008.
48. Xie, Y.; Zhang, Y.; Lan, H.; Mao, L.; Zeng, S.; Chen, Y.; Investigating long-term trends of climate change and their spatial variations caused by regional and local environments through data mining. J. Geogr. Sci. 2018, 28, 802-818. https://doi.org/10.1007/s11442-018-1506-9.
49. Feng, D.; Wang, J.; Fu, M.; Liu, G.; Zhang, M.; Tang, R.; Spatiotemporal variation and influencing factors of vegetation cover in the ecologically fragile areas of China from 2000 to 2015: A case study in Shaanxi Province. Environ. Sci. Pollut. R. 2019, 26, 28977-28992. https://doi.org/10.1007/s11356-019-06096-9.
50. Yin, S.; Guo, M.; Wang, X.; Yamamoto, H.; Ou, W.; Spatiotemporal variation and distribution characteristics of crop residue burning in China from 2001 to 2018. Environ. Pollut. 2021, 268, 115849. https://doi.org/10.1016/j.envpol.2020.115849.
51. Meng, N.; Wang, N. A.; Cheng, H.; Liu, X.; Niu, Z.; Impacts of climate change and anthropogenic activities on the normalized difference vegetation index of desertified areas in northern China. J. Geogr. Sci. 2023, 33, 483-507. https://doi.org/10.1007/s11442-023-2093-y.
52. Wang, X.; Qiu, B.; Li, W.; Zhang, Q.; Impacts of drought and heatwave on the terrestrial ecosystem in China as revealed by satellite solar-induced chlorophyll fluorescence. Sci. Total. Environ. 2019, 693, 133627. https://doi.org/10.1016/j.scitotenv.2019.133627.
53. Song, L.; Li, Y.; Ren, Y.; Wu, X.; Guo, B.; Tang, X.; Shi, W.; Ma, M.; Han, X.; Zhao, L.; Divergent vegetation responses to extreme spring and summer droughts in Southwestern China. Agr. Forest. Meteorol. 2019, 279, 107703. https://doi.org/10.1016/j.agrformet.2019.107703.
54. Qiu, R.; Li, X.; Han, G.; Xiao, J.; Ma, X.; Gong, W.; Monitoring drought impacts on crop productivity of the US Midwest with solar-induced fluorescence: GOSIF outperforms GOME-2 SIF and MODIS NDVI, EVI, and NIRv. Agr. Forest. Meteorol. 2022, 323, 109038. https://doi.org/10.1016/j.agrformet.2022.109038.
55. Yang, X.; Tang, J.; Mustard, J. F.; Lee, J. E.; Rossini, M.; Joiner, J.; Munger, J. W.; Kornfeld, A.; Richardson, A. D.; Solar-induced chlorophyll fluorescence that correlates with canopy photosynthesis on diurnal and seasonal scales in a temperate deciduous forest. Geophys. Res. Lett. 2015, 42, 2977-2987. https://doi.org/10.1002/2015GL063201.
56. Li, W.; Pacheco-Labrador, J.; Migliavacca, M.; Miralles, D.; Hoek van Dijke, A.; Reichstein, M.; Forkel, M.; Zhang, W.; Frankenberg, C.; Panwar, A.; Zhang, Q.; Weber, U.; Gentine, P.; Orth, R.; Widespread and complex drought effects on vegetation physiology inferred from space. Nat. Commun. 2023, 14, 4640. https://doi.org/10.1038/s41467-023-40226-9.
57. Du, L.; Mikle, N.; Zou, Z.; Huang, Y.; Shi, Z.; Jiang, L.; McCarthy, H. R.; Liang, Junyi.; Luo, Y.; Global patterns of extreme drought-induced loss in land primary production: Identifying ecological extremes from rain-use efficiency. Sci. Total. Environ. 2018, 628, 611-620. https://doi.org/10.1016/j.scitotenv.2018.02.114.
58. Liu, X.; Sun, G.; Fu, Z.; Ciais, P.; Feng, X.; Li, J.; Fu, B.; Compound droughts slow down the greening of the Earth. Global. Change. Biol. 2023, 29, 3072-3084. https://doi.org/10.1111/gcb.16657.
59. Ge, W.; Deng, L.; Wang, F.; Han, J.; Quantifying the contributions of human activities and climate change to vegetation net primary productivity dynamics in China from 2001 to 2016. Sci. Total. Environ. 2021, 773, 145648. https://doi.org/10.1016/j.scitotenv.2021.145648.
60. Liu, L.; Gudmundsson, L.; Hauser, M.; Qin, D.; Li, S.; Seneviratne, S. I.; Soil moisture dominates dryness stress on ecosystem production globally. Nat. Commun. 2020, 11, 4892. https://doi.org/10.1038/s41467-020-18631-1.
61. Zhong, Z.; He, B.; Wang, Y. P.; Chen, H. W.; Chen, D.; Fu, Y. H.; Chen, Y.; Guo, L.; Deng, Y.; Huang, L.; Yuan, W.; Hao, X.; Tang, R.; Liu, H.; Sun, L.; Xie, X.; Zhang, Y.; Disentangling the effects of vapor pressure deficit on northern terrestrial vegetation productivity. Sci. Adv. 2023, 9, eadf316. https://doi.org/10.1126/sciadv.adf3166.

 doi:10.20944/preprints202310.0075.v1